Published in GNSS 19th International Technical Meeting of the Satellite Division, 2383-2395, 2006
which should be used for any reference to this work

A flexible Galileo E1 Receiver Platform for the Validation of Low Power and Rapid Acquisition Schemes

C. Botteron, G. Wälchli, G. Zamuner, M. Frei, D. Manetti, F. Chastellain, P.-A. Farine
Institute of Microtechnology, University of Neuchâtel, Switzerland.
Patrice Brault, *Martec Serpe-Iesm, France.*

BIOGRAPHY

Dr Cyril Botteron received the Electronics Engineering degree in 1991 from the University of Applied Sciences in le Locle, Switzerland, and the PhD degree in 2003 from the University of Calgary in Canada. From 1991 to 2000, Cyril worked as electronics and software engineer for different companies in the USA, in Switzerland, and in Canada. Since 2003, Cyril is working as team leader for the Institute of Microtechnology (IMT) at the University of Neuchatel, leading different projects in collaboration with other R&D institutions and companies. His current research interests include radio frequency (RF) circuits and system designs with applications for indoor positioning using ultra-wideband technology, and outdoor positioning using GNSS and other terrestrial techniques. Cyril is also a senior member of the IEEE and a ION professional member.

ABSTRACT

With the inclusion of 406 MHz transponders on the Galileo satellites and the new search and rescue (SAR) return link message (RLM) on the open service E1B signal, the availability of distress beacons equipped with a Galileo or combined GPS/Galileo receiver will be very important in the future to take advantage of the SAR RLM, thereby facilitating the rescue operations and helping to identify and reject false alerts. Consequently, this paper provides the status of the development of a flexible Galileo L1 receiver platform as well as an analysis and comparison of acquisition schemes suitable to be implemented in 406 MHz Cospas-Sarsat distress beacons. For each considered acquisition scheme, we compare the acquisition performance that can be obtained using GPS L1 C/A or Galileo E1B or E1C signals and consider and discuss the following main constraints: a very short time to first fix (TTFF) in cold start conditions (the beacon's GNSS receiver may not be powered on for years before it is activated in an emergency); a low energy consumption per position fix (the beacon and GNSS receiver are battery powered); a possibly long coherent integration time to achieve synchronization and tracking in harsh environments (e.g., when some or all of the satellite signals are blocked or attenuated by an obstruction); the ability to demodulate the satellites signals in the presence of a 406MHz/5W and a 121.5MHz/(up to 100mW) beacon transmitters; and a low complexity (low price).

INTRODUCTION

To contribute to enhance the performances of the international Cospas-Sarsat SAR system, the Galileo satellites will broadcast globally the alert messages received from distress emitting beacons operating on the 406-406.1 MHz band, thereby allowing precise location of alerts (currently better than 1 nautical mile or 1.852km in 95% of the cases without GPS), multiple satellite detection to avoid terrain blockage in severe conditions, and near real-time reception of distress messages transmitted from anywhere on Earth (the average waiting time is currently one hour [1]). In addition, SAR/GALILEO will introduce a new SAR function, namely the return link from the SAR operator to the distress emitting beacon, thereby facilitating the rescue operations and helping to identify and reject false alerts [1].

As a beacon's GNSS receiver may not be powered on for years before it is activated in an emergency, one or more of the almanac, position and time parameters is very likely to be missing or obsolete. This means that the receiver will have to perform a cold start [2], i.e., search the sky for all possible PRN codes, in all possible Doppler bins, and for all 1023 (GPS L1C/A) or 4092 (Galileo L1B) code states of each PRN code until at least four SVs are acquired (note that even if a warm start would be possible, the specifications for COSPAS-SARSAT 406 MHz distress beacons require to force the beacon's internal GNSS receiver to perform a cold start [3]).

Since in an emergency the position of the receiver should be transmitted by the beacon as quickly as possible, a very fast acquisition architecture/algorithm yielding a very short TTFF in cold start condition is needed. In addition, since the beacon is battery powered, the selected acquisition architecture/algorithm should not consume too much power during the cold start acquisition as well as during the subsequent position fixes (the receiver should have the capability to provide one position fix every 20 minutes [3]). Additional constraints

for a GNSS receiver to operate in a distress beacon include the ability to demodulate the satellites signals (and decode the SAR RLM transmitted on Galileo E1B) in the presence of a 406MHz/5W and a 121.5MHz/(up to 100mW) beacon transmitters, and the ability to perform medium to long coherent integration times in order to achieve satellite signals acquisition and tracking in harsh environments (e.g., when some or all of the satellite signals are blocked or attenuated by an obstruction).

Based on this foreground, the following topics are addressed in this paper:

1. Description and development status of a flexible Galileo E1 receiver platform designed to develop and validate low power and rapid acquisition schemes suitable to be implemented in distress beacons.

2. Optimization of the number of partial correlations to minimize the losses due to a residual Doppler offset in a parallel FFT-based frequency search architecture.

3. Analysis of GPS L1 C/A and Galileo E1 B & C (see Table 1) signal acquisition performance in terms of received signal to noise ratio, mean probability of detection, and mean time of acquisition. The following different search architectures are considered in the analysis: serial search; parallel FFT-based frequency search; full Galileo BOC(1,1) acquisition; Galileo BOC(1,1) single lobe acquisition.

Signal Name	Modulation	Code Structure	Chip Rate	Symbol Rate	Carrier frequ.
GPS L1C/A	BPSK(1)	Gold 1023	1.023 Mcps	50 sps	1.575 MHz
Galileo OS L1B	BOC(1,1)	Memory 4092	1.023 Mcps	250 sps	1.575 MHz
Galileo OS L1C	BOC(1,1)	Tiered code 25×4092	1.023 Mcps	Data-free	1.575 MHz

Table 1 Main characteristics of GPS L1 C/A and Galileo L1B and L1C.

1 - DESCRIPTION AND DEVELOPMENT STATUS OF THE GALILEO E1 RECEIVER PLATFORM

In order to develop and validate low power and rapid acquisition schemes suitable to be implemented in distress beacons, we have developed a flexible Galileo E1 receiver platform composed of three main boards (see Fig. 1) and including: a) a custom built E1 radio frequency front-end board responsible for the signal downconversion; b) a commercial off-the-shelf PC/104 field programmable gate array (FPGA) board where the channel correlations and discrete Fourier transform (DFT) are hard coded for high-speed operations; c) a commercial off-the-shelf embedded platform for industrial computing (EPIC) processor board where the feedback control loops, filtering and discrimination algorithms are implemented to provide a maximum of flexibility.

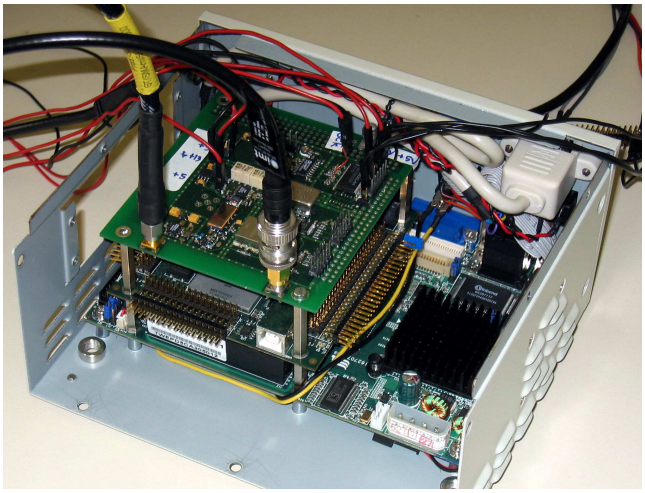

Fig. 1 Flexible Galileo E1 receiver platform.

The whole system consumes less than 10 W that can be supplied via an external 12 V power supply or 12 V battery. The above 3 units are discussed in more details in the next 3 subsections.

Radio Frequency Front-end Unit

The front-end is based on an heterodyne architecture. A passive antenna is used in order to be able to filter the signal before it reaches the low noise amplifier (LNA), which prevents the distress signals from overloading the front-end. Once filtered and amplified, the signal is downconverted to a first intermediate frequency (IF) at 70.14MHz where it is filtered by a SAW filter with a bandwidth of 5.5MHz. The signal is then downconverted by a quadrature mixer to a second IF at 4.758MHz, lowpass filtered and amplified by an amplifier with a -5dB to 40dB gain controlled digitally from the FPGA. The FPGA sets the gain in order to optimize the use of the subsequent 2 bits ADC. The sampling clock and the FPGA clock, 7.489MHz, are derived from the second oscillator. The complete frequency plan is shown in Fig. 2 (more details on the design and tests of the front-end unit are given in [4]).

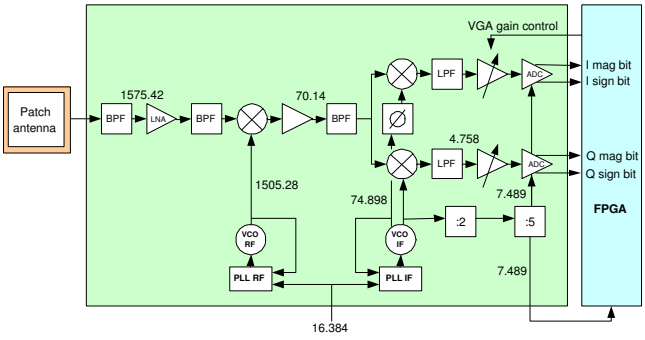

Fig. 2 Front-end frequency plan.

Microprocessor Unit

An "Ampro ReadyBoard 700 Pentium III EPIC Single Board System" that measures 115mmx165mm (4.5"x6.5") has been selected. This size is optimal for including full PC/104-Plus compliant expansion card (ISA and PCI buses) and a rich set of I/O implemented as either pin-headers or molded PC-style connectors (e.g., USB, serial & parallel, Ethenet ports, LC-Display, etc.). The whole system is passively cooled and equipped with a compact flash connector which allows replacing a conventional hard disc with a flash memory. This offers also a great advantage for updating the system, as a simple replacement of the compact flash allows bringing the whole system up-to-date. With this choice, the test bed is compact in size and equipped with absolutely no mechanical parts. The main application (acquisition and tracking) is running under DOS, allowing the full control of the running tasks or applications.

The microprocessor unit controls the baseband acquisition and tracking of the channels. In this manner, it is possible to easily implement, configure, and test different acquisition techniques, e.g., the serial search technique, the parallel frequency space search technique, or even the parallel code space search technique. These techniques are depicted in Fig. 3a-c and described below:

a) In the serial search acquisition, the bins of the 2-dimensional code-Doppler search space (see Fig. 4) are searched in a sequential or serial manner. The baseband input signal is first multiplied with the in-phase and quadrature signals corresponding to a given Doppler frequency bin, and then with the locally generated PRN signal corresponding to a given code phase bin. The resulting in-phase and quadrature signals are then integrated over a pre-detection integration time (PIT). The magnitude of the integrated in-phase and quadrature components are finally compared with a threshold to detect if a correlation peak has been found. If not, the next code phase or next frequency bin is searched.

b) In the parallel frequency space search acquisition, all possible Doppler bins are tested in parallel. The baseband input signal is first multiplied with a locally generated PRN code in order to form P successive partial correlations (also called partial complex matched filter operations (PCMF) in [5]). Then, the P results are combined using a complex N-points FFT (or DFT in practical FPGA implementations), where $N \geq P$ (if $N > P$, zero-padding is used). As the partial correlations are P times smaller than the PIT, all the Doppler frequencies can be searched in parallel (assuming that P is chosen correctly) and the largest magnitude of the N FFT bins is compared to a threshold to detect if a correlation peak has been found. If not, the operation is repeated for the other code phases until the correlation peak has been found.

c) In the parallel code space acquisition, all possible code phases are tested in parallel. The input signal is first multiplied with the in-phase and quadrature signals. Then, the resulting signals are transformed via FFT. The locally generated PRN code is also transformed via FFT, and the complex conjugated values of the coefficients are computed. After multiplying these two sets of coefficients (correlation in the frequency space), the inverse FFT coefficients and their energies are computed in order to determine if a correlation peak has been found. If not, another frequency bin is searched by shifting the FFT components of the locally generated PRN code.

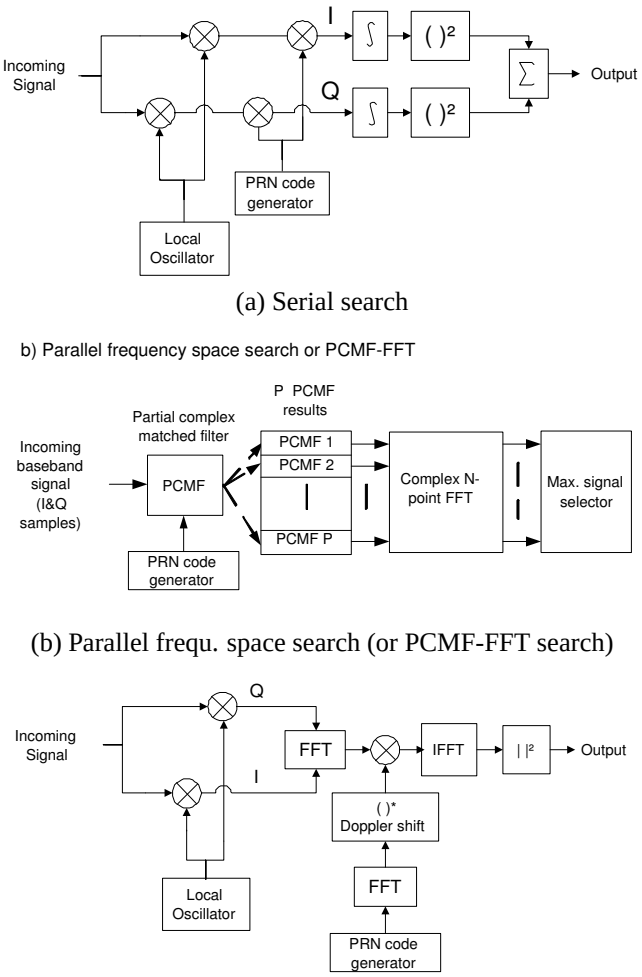

(a) Serial search

(b) Parallel frequ. space search (or PCMF-FFT search)

(c) Parallel code space search

Fig. 3 Different acquisition techniques.

Remark: as in general the number of code phase bins is much greater than the number of frequency bins, a parallel code space acquisition will provide the shortest TTFF by searching at once all the code phase bins for every frequency bin instead of all the frequency bins for every code phase bin as in the parallel frequency search. However, it will also require a very large FFT size which implementation on today's CMOS technologies would certainly be prohibitive with the size, memory and power requirements of a low power and low cost distress beacon application. Consequently, we will only focus for the rest of this paper on the serial and parallel frequency space search acquisition architectures that are

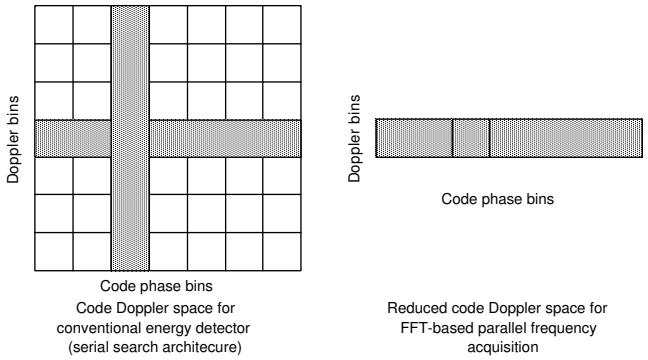

Fig. 4 2-dimensional code-Doppler space.

compatible with a low implementation complexity.

FPGA Base Band Processing Unit

A Nova Constallation-20KE FPGA card featuring an Altera APEX 672-Pin FPGA device and ISA interface compatibility has been selected to implement 12 acquisition and tracking channels controlled by a microprocessor unit (see Fig. 5).

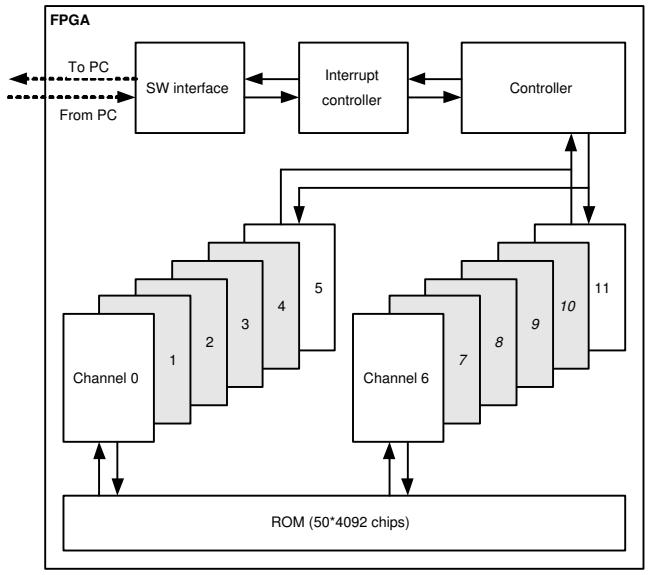

Fig. 5 Simplified schematic of the base band processing unit (FPGA Unit).

Unlike the GPS L1 C/A PRN codes, the Galileo E1 B and C PRN codes can not be automatically generated and must therefore be pre-programmed in a memory. As the FPGA incorporates dedicated enhanced embedded system blocks (so called ESBs) supporting memory structures, the totality of the 50 PRN codes are stored in a global ROM accessible from every channel. When a new channel is activated, or a new code selected, the desired PRN code is automatically downloaded from the system ROM to the local RAM of the respective channel. This way, each channel can access independently and locally its own code, avoiding system conflicts. In addition to the RAM for local PRN code storage, each channel embeds two independent 32 bits NCO (carrier and code) with sine and cosine maps, carrier mixers and integrate & dump units (see Fig. 6).

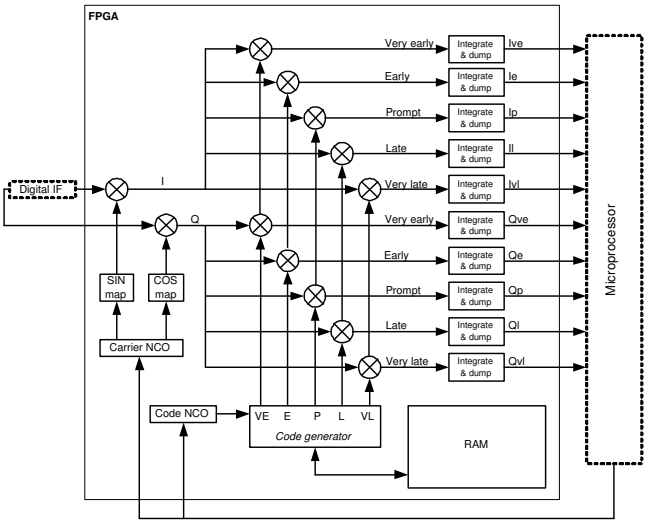

Fig. 6 Simplified schematic of one base band channel.

To acquire the Galileo BOC(1,1) signal, two acquisition architectures have been considered for implementation, namely "full BOC(1,1) acquisition" and "BOC(1,1) single lobe acquisition":

1) Full BOC(1,1) acquisition:

Due to the square wave sub-carrier modulation introduced in Galileo E1 BOC(1,1), the autocorrelation presents a sharper main peak (as compared to GPS L1 C/A BPSK(1)) and two small negative sides peaks (see Fig.7). This has the following important implications:

- A sharper correlation peak allows for a better pseudo-range estimation, a better multipath mitigation, and thus a better positioning accuracy. Unfortunately, a high positioning accuracy is not required for beacon applications since the transmitted positioning accuracy is limited to 4 seconds (corresponding to about 120 meters) due to resolution of coding in the SAR Cospas Sarsat 406 MHz beacon long message [3]).

- Due to the sharper correlation peak (3 times sharper than BPSK(1)'s), a smaller code step size must be used during the acquisition phase (3 times smaller to yield a similar performance). If not, the worst case loss occurring when the received BOC(1,1) code phase falls between two code bins can be very high, e.g., $20log_{10}(1 - 3 \times 0.25) \approx -12$dB for a 1/2 chip code step size as compared to only $20log_{10}(1 - 0.25) \approx -2.5$dB for a BPSK(1) peak.

- In terms of search complexity, a sharper correlation peak is obtained at the cost of a higher sampling rate ($\propto 1/$width of autocorrelation function) and a smaller code step size ($\propto 1/$width of autocorrelation function), resulting in a quadratic increase in search complexity

($\propto 1/\{$width of autocorrelation function$\}^2$) or equivalently in a longer TTFF if the complexity is restricted to be the same.

- The multiple peaks of the autocorrelation function induce an increased complexity in the acquisition phase to avoid selecting and tracking one of the two side peaks sitting 1/2 chip away from the main peak, as this would introduce an important ranging error (1/2 chip corresponds to about 146.6 meters).

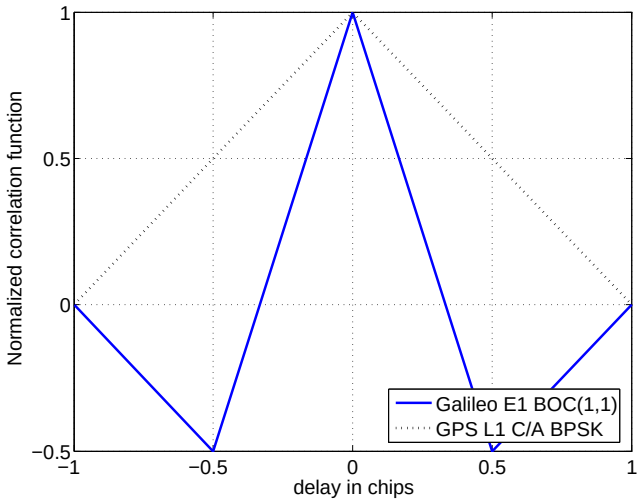

Fig. 7 Normalized correlation function of GPS L1 C/A (BPSK(1)) and Galileo E1 (BOC(1,1)).

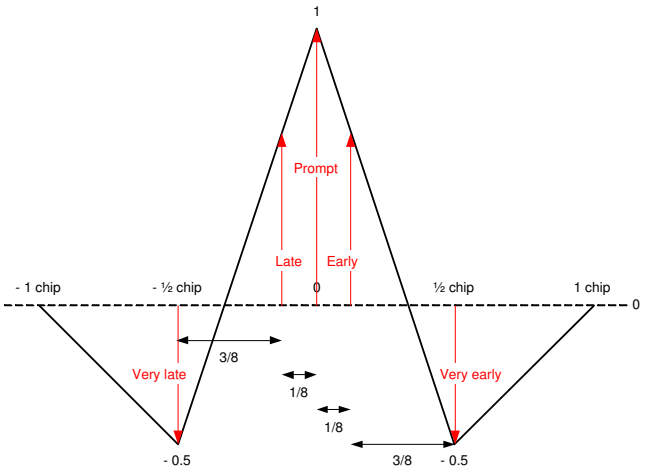

Fig. 8 Example of T_{shift} organization in tracking mode corresponding to a spacing of 3/8 - 1/8 - 1/8 - 3/8 chip.

In order to select and track the correct BOC(1,1) peak, we have implemented in our design five replicas of the code referenced as Very early, Early, Prompt, Late and Very late (see Fig. 6). These replicas can be generated with a variable time shift T_{shift} at the frequency provided by the code NCO (see Fig. 8). The time T_{shift} separating two consecutive replicas is controlled via software and can be adjusted in real time. This can be useful to experiment with different step size increments or when going from acquisition to tracking phase.

2) Single lobe BOC(1,1) acquisition:

This technique (also called "BPSK like" method of acquisition [6]) considers the received BOC(1,1) signal as the sum of two BPSK(1) signals with carrier frequency symmetrically positioned on each side of the BOC carrier frequency. Each side lobe can thus be treated independently as a BPSK(1) signal (see Fig.9), which has the following implications:

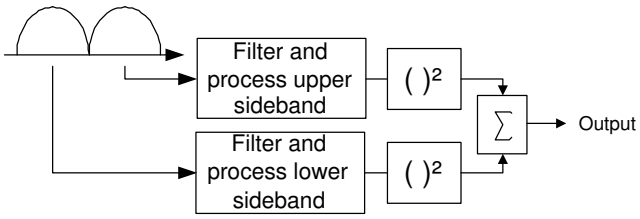

Fig. 9 Single lobe acquisition or BPSK like technique.

- The single side lobe correlation function has no side peaks and is symmetrical. However, the single lobe acquisition technique induces 3dB degradation in signal to noise ratio (SNR) if applied on a single side lobe (due to mismatch between local BPSK(1) and received BOC(1,1) codes) [6]. The 3dB loss can only be partially compensated if both lobes are processed in parallel and the two channel energies summed before the threshold test because of the additional degradation in the non-coherent combining integration.

- The search complexity on each side lobe is similar to BPSK(1) search complexity with an equivalent code length. The code step size during the acquisition phase can thus be reduced from 1/6 chip to 1/2 chip.

- Due to the narrowed spectrum, the positioning accuracy will be lower than with full BOC(1,1) acquisition. However, as discussed above, this may not be an issue for a SAR beacon receiver due to the relatively low requirements on transmitted positioning accuracy. Note also (for other applications) that it is still possible once the non-ambiguous BPSK-like peak has been detected to shift the receiver to nominal full BOC tracking.

Development Status

The development of the Galileo E1 receiver platform started on Nov. 17th and is now approaching completion. All the individual parts (front-end, baseband, software) of the Galileo receiver have been individually tested and the implementation and testing of the acquisition and tracking loops is now in progress.

The test and validation of the Galileo E1 receiver is performed using a Spirent GSS 7800 12 channels E1 simulator (see Fig. 10).

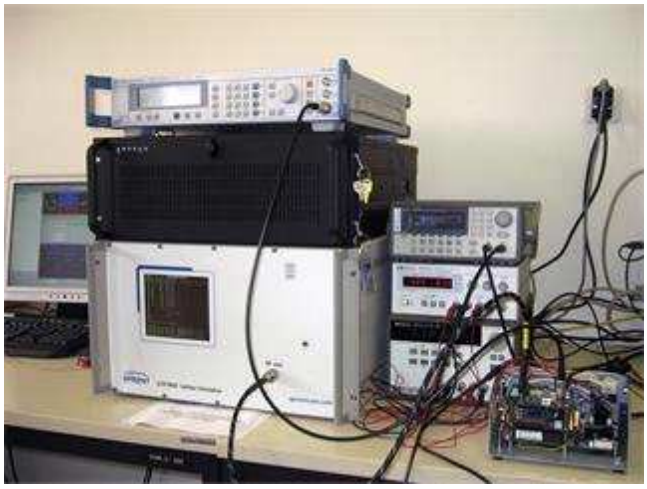

Fig. 10 Test and validation of the Galileo E1 receiver platform using Spirent GSS 7800 12 channels E1 Galileo simulator.

2 - OPTIMIZATION OF THE PARALLEL FREQUENCY SEARCH ARCHITECTURE

The presence of a Doppler offset f_D will degrade the coherent integration gain that can be achieved by a parallel frequency search FFT-based architecture (or PCMF-FFT architecture). Denoting $w_d \stackrel{\text{def}}{=} \pi f_D T_c$, where T_c denotes the chip period, the normalized PCMF-FFT correlation gain can be expressed as a function of the output bin k and residual Doppler frequency f_D as [5]

$$G_{PCMF-FFT}(f_D, k_{bin}) = \frac{1}{M}\left|\frac{\sin(w_d M/P)}{\sin(w_d)}\frac{\sin(w_d M - \pi P k_{bin}/N)}{\sin(w_d M/P - \pi k_{bin}/N)}\right| \quad (1)$$

where M denotes the total PIT converted in chips, i.e., $M = PIT/T_c$. Equ. (1) can also be written as the product of two terms, i.e., as

$$G_{PCMF-FFT}(f_D, k_{bin}) = \left|\frac{P\sin(w_d M/P)}{M\sin(w_d)}\right|\left|\frac{\sin(w_d M - \pi P/N k_{bin})}{P\sin(w_d M/P - \pi k_{bin}/N)}\right|. \quad (2)$$

As an illustration example, Fig. 11a shows the frequency response for a PCMF-FFT architecture using 16-PCMF outputs fed to a complex 16-pts FFT and assuming a PIT of 1ms ($M = 1023$ chips).

We can make the following observations:

- The first term of (1) represents the reduction of the coherent gain or correlation loss present at the output of the PCMF. It corresponds to the overall envelope shown with the continuous blue line in Fig. 11a. The search bandwidth at the output of the PCMF can be calculated as $\approx \frac{2P}{3PIT}$ (this yields a maximum correlation loss of $20\log_{10}(\text{sinc}(1/3)) = -1.6dB$). For example, in the considered example, the search bandwidth is $\approx \pm 5.3kHz$ (i.e., a total of 10.6 kHz). We note that the search bandwidth can be increased by increasing P and thus decreasing the partial correlation durations PIT/P. If a larger search bandwidth is not needed, increasing P can also be used to reduce the correlation loss at the output of the PCMF.
- The second term of (1) represents the additional losses (called scalloping losses) within the k_{bin}th FFT frequency bin. The worst scalloping losses occur when the Doppler frequency falls between two FFT bins (see black dashed line in Fig. 11b). Note that the scalloping losses can be reduced by using some zero padding prior computing the FFT [5]. This is illustrated in Fig. 11c where a padded FFT of size 32 has been used with the same number of PCMF as in Fig. 11b (i.e., 16-PCMF) to reduce the scalloping losses at the expense of a two times larger complex FFT.

Optimal PCMF-FFT configurations

Ideally, the detector's frequency response should be uniform for all frequencies and equal to the frequency response for $f_D = 0$ Hz. By changing the number of PCMFs and the FFT size, it is possible to "tune" the PCMF-FFT detector's frequency response such as to maximize the detector's output according to an a-priori probability density function (pdf) for the Doppler offsets $p_F(f)$. Thus, we want to find P such as the frequency response averaged over the Doppler frequency distribution is maximized, i.e.,

$$P = \max_P \left(\int_{-\infty}^{\infty} \hat{G}_{PCMF-FFT}(f) p_F(f) df\right) \quad (3)$$

where $\hat{G}_{PCMF-FFT}(f)$ denotes the envelope of $G_{PCMF-FFT}(f)$.

While the Doppler offset distribution will not be completely uniform even for a stationary user (the satellite will be at the zenith a shorter time than at the horizon), we can still approximate it with a uniform distribution as $p_F(f) = U[-5, 5]$ kHz (valid for a stationary user) to obtain the optimal values for P assuming different FFT sizes and PITs (see Table 2). We note that P and N have to be increased for increasing PIT. This is because the overall frequency response

PIT ms	N-FFT	$P-$PCMF	MT_c ms	$\frac{MT_c}{P}$ us	$\frac{1}{2}\frac{2P}{3MT_c}$ Hz	min G
1	16	13	1.001	77	$\pm$ 4500	0.56
1	32	17	1.003	59	$\pm$ 4500	0.62
4	64	51	3.978	78	$\pm$ 4875	0.54
4	128	71	3.976	56	$\pm$ 4875	0.61
10	128	114	10.032	88	$\pm$ 4950	0.49
10	256	160	10.08	63	$\pm$ 4950	0.60

Table 2 Example of optimal PCMF-FFT configurations and min. achievable normalized correlation gain for a frequency search space of $\pm$5kHz and various PITs.

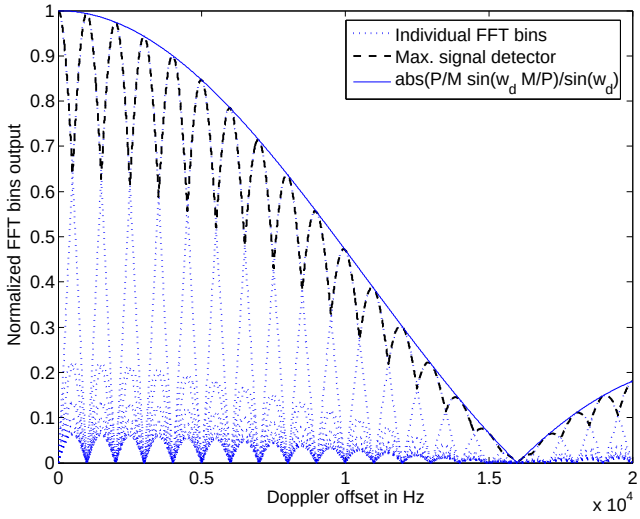

(a) $P = 16$-PCMF; $N = 16$-pts FFT

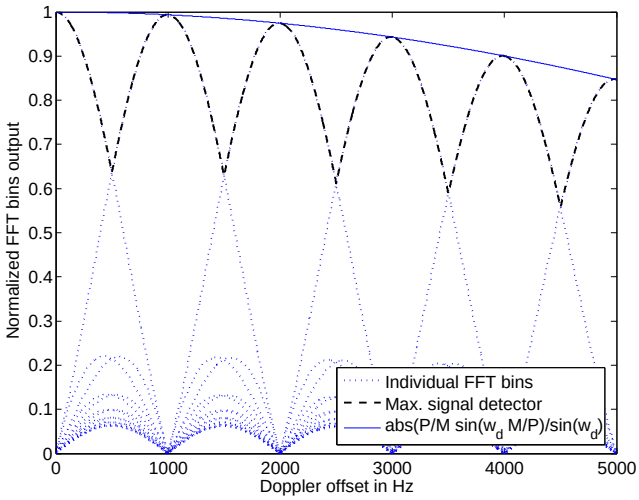

(b) $P = 16$-PCMF; $N = 16$-pts FFT

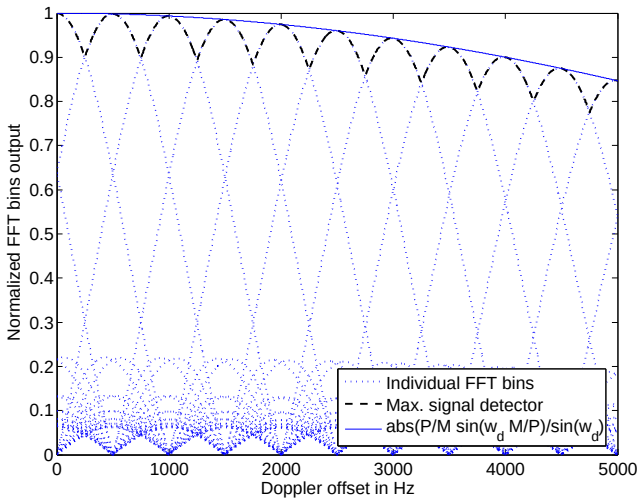

(c) $P = 16$-PCMF; $N = 32$-pts FFT

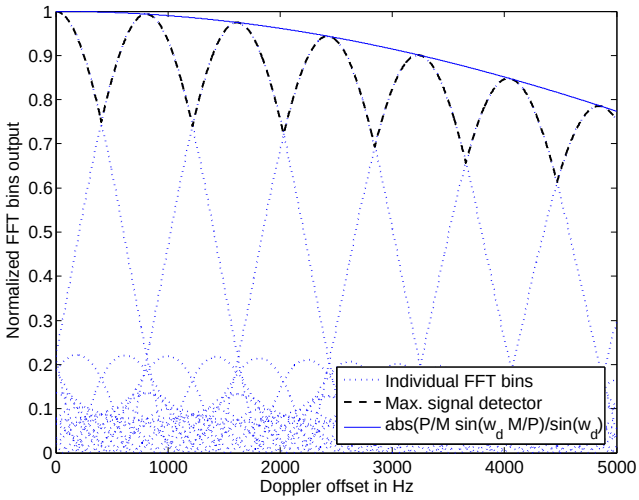

(d) $P = P_{opt} = 13$-PCMF; $N = 16$-pts FFT

Fig. 11 Frequency response for a P-PCMF receiver using a N-pts FFT for a PIT of 1ms ($M = 1023$ chips)

is shaped with $\left|\frac{P\sin(w_d M/P)}{M\sin(w_d)}\right|$. Thus, if we increase M to increase the PIT, we should also increase P proportionally not to have a reduction in sensitivity too important (as a rule of thumb, P should thus be chosen such that $\frac{2P}{3MT_c}$ is not much less than the desired search bandwidth. However, it is better to use (3) to find the optimal value for P).

As an illustration example, Fig. 11d shows the frequency response for a PCMF-FFT architecture using 13-PCMF outputs fed to a 16-pts FFT and assuming a PIT of 1ms ($M = 1023$ chips).

Remark: in comparison with Fig. 11b, we note that while the overall frequency response given by the first term of (1) is a little lower at high frequencies, all the scalloping losses have been greatly reduced. Thus, assuming no a-priori information about the Doppler offset (e.g., the whole Doppler space has to be searched between $\pm$5kHz), this configuration using a lower number of PCMFs (13 instead of 16) will provide better overall performance than the initial configuration with $P = 16$ for the same FFT size and PIT.

Remark Concerning the Conventional Serial Search

For a conventional serial search energy detector, $P = N = 1$, and (1) simplifies as

$$G_{CMF}(f_D) = \frac{1}{M}\left|\frac{\sin(w_d M)}{\sin(w_d)}\right| \approx \left|\frac{sin(w_d M)}{w_d M}\right|, w_d \ll 1 \quad (4)$$

In this particular case, the search bandwidth is similar to the one produced by a single FFT bin ($\approx \frac{2}{3PIT}$), which gives $\approx \pm 333Hz$ for a PIT of 1ms. Consequently, the search must be performed successively over various Doppler frequency offsets or frequency bins. Table 3 gives examples of possible serial search configurations.

PIT ms	search BW $\frac{2}{3MT_c}$[Hz]	F_{bins} = nb. of frequ. bins	min G
1	667	15	0.83
4	167	60	0.87
10	67	150	0.77

Table 3 Example of possible serial search configurations and min. achievable normalized coherent correlation gain for a frequency search space of ± 5kHz and various PITs.

3 - ANALYSIS OF GPS L1 C/A AND GALILEO E1 B AND C SIGNAL ACQUISITION PERFORMANCE

Signal to Noise Ratio (SNR) Comparison

From the Galileo and GPS signal in space interface documents (see [7] and [8]), the minimum received power at 10° elevation into a 0dBi antenna is -131.3dBm for GPS L1 C/A and -127dBm for Galileo E1 B and C (the power sharing between Galileo pilot and data channels is of 50%). Assuming a receiver bandwidth of 2 MHz and 4 MHz for GPS and Galileo signals, respectively, and a receiver noise figure of 3dB, the SNR at the input of the correlators (i.e., before coherent integration) will be of -23.3dB and -25dB for GPS L1 C/A and Galileo E1B or E1C, respectively, as shown in Table 4.

	GPS L1 C/A	Galileo E1 B or E1 C
Min. rx. power [dBm]	-131.3	-127-3=-130
Th. noise BW [MHz]	2	4
Th. noise level [dBm]	-174+63=-11	-174+66=-108
Rx. noise figure [dB]	3	3
Resulting SNR [dB]	-131.3-(-111+3) =-23.3	-130-(-108+3) =-25
Resulting C/No [dB/Hz]	39.7	41

Table 4 GPS L1 C/A and Galileo E1 minimum signal levels at 10° elevation into a 0dBi antenna and assuming a 3dB receiver noise figure.

Remark: despite the fact that the Galileo signals (data E1B or pilot E1C) are received with a 1.3dB higher power at the antenna, the GPS L1 C/A signal provides a 1.7dB higher SNR than the Galileo data (E1B) or pilot (E1C) signals due to the narrower receiver noise bandwidth. The only way for the Galileo E1 signal to provide a SNR advantage would be if the data and pilot channels were combined at the receiver (this would provide a 1.3dB advantage for Galileo E1 at the expense of a higher receiver complexity).

Detection and False Alarm Probabilities

Let us assume that the noise at the input of the PCMF correlator (see Fig. 3b) is zero-mean Gaussian distributed with variance σ^2. If the partial correlation M/P is sufficiently long, then from the central limit theorem (CLT) the noise at the output of the PCMF correlator will be zero mean with variance $\sigma^2 M/P$. Assuming P PCMFs, the output of a complex zero-padded FFT of length N ($N \geq P$) will have variance $P\sigma^2 M/P = \sigma^2 M$ (the uncorrelated assumption that is used here may not be fully valid with a zero padded FFT, but is used to simplify the derivation).

In the absence of signal, The magnitude of the FFT that are used in the detector will be Rayleigh distributed according to (see, e.g. [9])

$$p_Y(y) = \frac{y}{\sigma^2 M} e^{-\frac{y^2}{2\sigma^2 M}}, y \geq 0. \quad (5)$$

The probability that a FFT output be greater or equal than a given threshold t is thus

$$P[output_k > t]|_{\text{no signal}} = 1 - F_Y(t) = e^{\frac{-t^2}{2\sigma^2 M}} \quad (6)$$

where $F_Y(y)$ denotes the cumulative density function (cdf) of Y.

The probability of false alarm is the probability that one or more FFT output is greater than the threshold. It can be written as

$$\begin{aligned} P_{fa} &= 1 - (1 - P[output_k > t]|_{\text{no signal}})^N \\ &= 1 - \left(1 - e^{-\frac{t^2}{2\sigma^2 M}}\right)^N. \end{aligned} \quad (7)$$

In order to compare the performance of different acquisition architectures, we will fix P_{fa} and calculate the threshold to reach the desired P_{fa}. In this case, we can rewrite (7) to find the corresponding threshold as

$$t(P_{fa}) = \sqrt{-2\sigma^2 M \ln\left(1 - (1 - P_{fa})^{1/N}\right)} \quad (8)$$

If we now assume that a signal is present at the kth output of the FFT, the magnitude of the FFT bin will be Ricean distributed with the following cdf (see, e.g. [9])

$$F_{Y_k}(y_k) = 1 - Q\left(\frac{s_k}{\sqrt{\sigma^2 M}}, \frac{t}{\sqrt{\sigma^2 M}}\right), y_k \geq 0 \quad (9)$$

where $Q(\cdot,\cdot)$ denotes the Markum Q function and s_k^2 denotes the summation of the mean square amplitude on the inphase and quadrature FFT banches of the kth FFT output, i.e., $s_k^2 = m_I^2(k) + m_Q^2(k)$. Note that the amplitudes $m_I(k)$ and $m_Q(k)$ at the output of the kth FFT bin will depend on the input SNR as well as on the Doppler frequency offset through (1).

The probability that the amplitude of bin k is greater than the threshold t in the presence of a signal is thus

$$P[output_k > t]_{\text{signal}} = Q\left(\frac{s_k}{\sqrt{\sigma^2 M}}, \frac{t}{\sqrt{\sigma^2 M}}\right). \quad (10)$$

Finally, as a signal will be detected if one or more FFT bin output is greater than the threshold, the probability of detection can be computed as

$$\begin{aligned} P_{d,1peak} &= 1 - \prod_{k=0}^{N} \{1 - P[output_k > t]_{\text{signal}}\} \\ &= 1 - \prod_{k=0}^{N} \left\{1 - Q\left(\frac{s_k}{\sqrt{\sigma^2 M}}, \frac{t}{\sqrt{\sigma^2 M}}\right)\right\} \end{aligned} \quad (11)$$

Remarks:

- Equ. (11) is not valid at low SNR if a full BOC(1,1) acquisition method is used due to the presence of the two side peaks that will increase the likelihood of detection (see Fig.12). In order to take the side peak detection into account, we first calculate the probability of detecting one of the two side peaks as

$$P_{d,s2} = 2P_{d,s} - P_{d,s}^2 \tag{12}$$

where $P_{d,s}$ is the probability of detection of a single side peak that can be calculated using (11) with s_k replaced by $s_k/2$ (the side peak amplitude is half the main peak amplitude). The probability of detection in the presence of the BOC(1,1) side peaks is now the probability of either detecting one of the 2 side peaks or the main peak and can thus be written as

$$P_{d,BOC(1,1)} = P_{d,1peak} + P_{d,s2} - P_{d,1peak}P_{d,s2}. \tag{13}$$

- In the presence of a Doppler offset, s_k will be reduced according to (1), and the probability of detection will thus be smaller. In order to include the effect of Doppler effects in the computation of the mean time of acquisition, we can consider the probability of detection given in (11) or (13) as a conditional probability for a given Doppler frequency offset, and average it over the pdf of the Doppler offset distribution $p_F(f)$. We then obtain

$$\begin{aligned} E[P_{d,1peak}] &= \int_{-\infty}^{\infty} P_{d,1peak}(f)p_F(f)df \\ E[P_{d,BOC(1,1)}] &= \int_{-\infty}^{\infty} P_{d,BOC(1,1)}(f)p_F(f)df. \end{aligned}$$

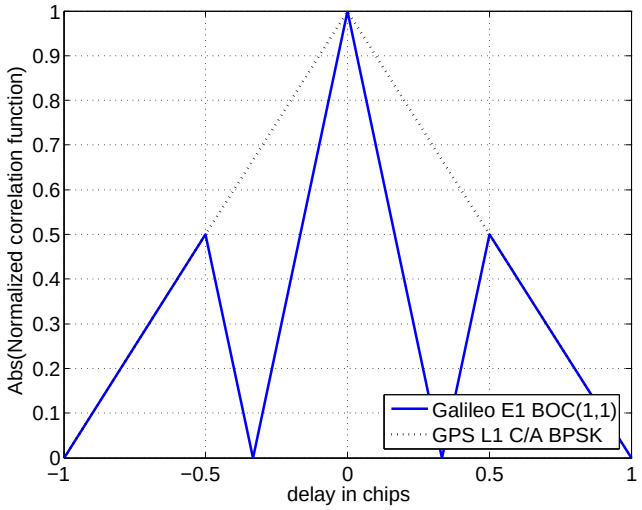

Fig. 12 Normalized absolute correlation function of GPS L1 C/A and Galileo BOC(1,1)

Mean Time of Acquisition

The mean time of acquisition and its variance for a single dwell time system has already been derived for a conventional energy detector [10] and can be readily adapted at the problem at hand as

$$E[T_{acqu}] = \frac{(2-P_d)(1+KP_{fa})}{2P_d} T_{bins}F_{bins}PIT \tag{14}$$

where PIT is the dwell time in seconds, T_{bins} is the total number of phase bins to be searched, F_{bins} is the total number of frequency bins to be searched ($F_{bins} = 1$ for the parallel frequency space search), and K is the penalty factor representing the number of PIT periods that are lost while trying to track the signal upon a false detection.

Presentation and Discussion of the Results

Note that the aim of this section is not to present some quantitative results, but more to present qualitative results that illustrate the trade-offs in selecting different signals (e.g., GPS L1 C/A vs. Galileo E1 B) and different acquisition architectures (e.g., serial vs. parallel, or BOC(1,1) single lobe vs. full BOC(1,1)).

In order to provide generalized results that can be applied to different situations, we compute the prob. of correlation peak detection and mean time of acquisition as a function of the C/No and normalize them with the total time required to search all the code phases, i.e., by the product of the PIT and the number of code phase cells T_{bins}.

In this way, it is possible to apply the results to the GPS L1 C/A and Galileo BOC(1,1) signals by considering their corresponding $T_{bins}PIT$ products (see Table 5 for some typical values).

Note that the minimum normalized mean time of acquisition is $0.5F_{bins}$ (as can be verified by setting $P_{fa} = 0$ and $P_d = 1$ in (14)).

PIT	Tot. code phase search time:$T_{bins}PIT$		
ms	GPS L1 C/A	Galileo BOC(1,1)	
		Single lobe	Full BOC(1,1)
	$T_{bins} = 2046$	$T_{bins} = 8184$	$T_{bins} = 24552$
1	≈ 2.0s	≈ 8.2s	≈ 24.6s
4	≈ 8.2s	≈ 32.7s	≈ 98.2s
10	≈ 20.5s	≈ 81.8s	≈ 245.5s

Table 5 Time to search all the code phase bins for different PITs.

Effect of zero padding and optimum number of PCMFs:

Fig.13 illustrates the improvement in probability of detection and mean time of acquisition for the parallel frequency space search architecture obtained by optimizing the number of PCMF for a PIT of 1ms and a 32-pts FFT size. We note that with $P = 17$, the results obtained for the worst Doppler offset as well as the results averaged over the distribution of the Doppler approach the ideal results with zero Doppler offset. We also note that at very low and very high SNR the Doppler offset has no influence on the results. This is because the detection probability is dominated by the noise level and the signal level at very low and very high SNR, respectively.

C/No	Normalized mean time of acquisition $E[T_{acqu}]/(T_{bins}PIT)$											
	PIT=1ms				PIT=4ms				PIT=10ms			
	single lobe BOC or BPSK(1)		full BOC(1,1) &side peaks		single lobe BOC or BPSK(1)		full BOC(1,1) &side peaks		single lobe BOC or BPSK(1)		full BOC(1,1) &side peaks	
	P13N16	SER	P13N16	SER	P51N64	SER	P51N64	SER	P114N128	SER	P114N128	SER
20	19	277	6	94	19	1017	6	360	19	2177	6	824
25	19	261	6	92	19	832	6	323	18	1446	6	648
30	18	222	6	84	18	515	6	242	17	656	6	379
35	16	147	6	66	14	217	5	132	9	232	4	183
40	11	67	5	39	5	79	3	67	2	150	1	150
45	4	24	3	19	1	60	1	60	1	150	1	150
50	1	15	1	15	1	60	1	60	1	150	1	150
55	1	15	1	15	1	60	1	60	1	150	1	150
60	1	15	1	15	1	60	1	60	1	150	1	150

Table 6 Normalized mean time of acquisition for a frequency search space of $\pm$5kHz; $P_{fa} = 0.1$; and K=10.

Effect of the penalty factor K:

Fig. 14 illustrates the effect of the penalty factor K on the mean time of acquisition of a parallel frequency space search architecture and assuming a PIT of 1ms (similar results can be observed for the serial search architecture or longer PITs). We note that at high C/No, the mean time of acquisition does not improve anymore with the C/No due to the penalty factor and assumed constant false alarm rate. We also note from Fig. 14b that if the selected P_{fa} is very low, the mean time of acquisition at very low C/No is degraded (a very low P_{fa} means a very high detection threshold t), while at high SNR is it improved (a lower P_{fa} means less false alarm penalty). This means that the P_{fa} and thus the detection threshold should be set to a different value depending on the a-priori information available about the C/No to yield a good trade off between a very high and very low mean time of acquisition at low and high C/No, respectively.

Effect of the BOC(1,1) side peaks:

On Fig. 15 and Fig. 16 we plotted the probability of detection and mean time of acquisition for a single correlation peak (representative of GPS L1 C/A or Galileo E1 single lobe acquisition) as well as the full BOC(1,1) multiple correlation peaks (representative of Galileo E1 full BOC(1,1) acquisition), for the parallel frequency search and serial search, respectively. We note that as expected the normalized probability of detection (and consequently the mean time of acquisition) is improved at low C/No. On the other hand, at high C/No, the correlation main peak is rising well above the noise floor and the presence of the side peaks does not improve the detection probability.

Comparison of GPS BPSK(1) and Galileo BOC(1,1) acquisition:

By looking at Fig. 15-16 and Table 6, we can make the following observations:

- The improvement in normalized probability of detection that is observed when considering Galileo E1 full BOC(1,1) acquisition instead of BOC(1,1) single lobe acquisition is always less than 3 (since there are only 3 peaks and the 2 side peaks have half the amplitude of the main peak). Consequently, even at low C/No, this improvement does not compensate for the 3 times larger number of code phase cells that must be searched if a full BOC(1,1) acquisition architecture is chosen (see T_{bins} in Table 5).

- Note that even if we consider the fact that there will be a 3dB degradation in SNR when using the BOC(1,1) single lobe acquisition technique, the above remark remains true (although the detection performance of both techniques will be similar over a short C/No range in the 40-45dB/Hz region).

- Based on the above two remarks, the single lobe acquisition technique seems a good choice to acquire the Galileo E1 B or C signal with a low implementation complexity. As already discussed, this is especially true for a distress beacon GNSS receiver where a high accuracy is not needed.

- If we now compare Galileo E1 BOC(1,1) single lobe acquisition with GPS L1 BPSK(1) acquisition, the normalized mean time will be the same. However, we note from Table 5 that the absolute mean time of acquisition will be 4 times shorter using GPS L1 C/A rather than Galileo E1 (GPS L1 C/A uses a 4 times shorter code length).

- Comparing the parallel frequency search method with the serial search method, we note that the mean time of acquisition for the former method can be as much as F_{bins} times faster, where F_{bins} denote the number of frequency bins for the serial search (see Table 3). The reduction in TTFF using the parallel frequency space search method becomes particularly important with long PITs (e.g., a reduction of 150 times for a PIT of 10ms while only requiring a relatively small FFT size ($N = 128$ pts).

CONCLUSIONS

In this paper we have described a flexible Galileo E1 receiver prototype used to validate different low power and rapid acquisition schemes. As the cold start TTFF performance is very important for a distress beacon application, we have conducted a theoretical analysis of different acquisition architectures and compared their performance when using GPS L1 C/A and Galileo E1 B or E1 C signals.

The main observations we obtained are the following: 1) If a parallel FFT-based frequency search architecture is used, selecting the optimum number of PCMF with the method provided in this paper can greatly reduce the losses due to the Doppler offsets. 2) A parallel FFT-based frequency search architecture can greatly reduce the TTFF and/or provide an increased sensitivity while only requiring a modest increase in implementation complexity (due to the addition of the DFT). 3) As a distress beacon's required positioning accuracy is not very high, a single lobe acquisition method to acquire the Galileo E1 BOC(1,1) seems the best choice (offering a quadratic reduction in implementation complexity as compared to full BOC(1,1) acquisition). 4) Acquiring the Galileo E1 BOC(1,1) requires more complexity than acquiring GPS L1 C/A to obtain a similar TTFF (the larger received power on Galileo E1 and the improved detection probability with the full BOC(1,1) acquisition method do not compensate for the longer code length). 5) For a distress beacon, it may well be more efficient (in terms of speed, computational power) to first acquire GPS L1 C/A signal in cold start prior to acquire Galileo E1B signal in warm or hot start.

While our work has focused at the Cospas-Sarsat distress beacon application, the results we obtained are still valid for any other low power application requiring a very short TTFF in cold start conditions, a low implementation complexity, and a good sensitivity.

ACKNOWLEDGMENTS

This work was partially conducted in the frame of the project GRDB (Galileo Receiver for Distress Beacon) that is partially financed by the Galileo Joint Undertaking (GJU) in the frame of the GJU second call area 3 under the 6th Framework Program of the European Commission. This support is greatly acknowledged.

REFERENCES

[1] www.ec.europa.eu, *Search and Rescue Service (SAR)*, `http://ec.europa.eu/dgs/energy_transport/galileo/programme/service_sar_en.htm`.

[2] Kaplan E.D, *Understanding GPS Principles and Applications*, Artech House Publishers, Boston, London, 1996.

[3] Cospas-Sarsat, "Specification for COSPAS-SARSAT 406 MHz distress beacon," *C/S T.001 Issue 3 - revision 7*, nov 2005.

[4] F. Chastellain, C. Botteron, G. Waelchli, G. Zamuner, D. Manetti, P.-A. Farine, P. Brault, "A Galileo E1 RF Front-end Optimized for Narrowband Interferers Mitigation," in *ION GNSS 2006*, sep 2006.

[5] Spangenberg S.M., Scott I., McLaughlin S., Povey G.J.R., Cruickshank D.G.M., Grant P.M., "An fft-based approach for fast acquisition in spread spectrum communication systems," *Wireless Personal Communications*, vol. 13, no. 1-2, pp. 27–55, May 2000.

[6] Martin N., Leblond V., Guillotel G., Heiries V., "BOC(1,1) signal acquisition techniques and performances," in *ION GNSS 2003*, sep 2003, pp. 188–198.

[7] GALILEO-OS-SIS-ICD, "Galileo open service signal in space interface control document," *GAL OS SIS ICD/D.0*, 2006, Draft 0.

[8] IS-GPS-200D, "Navstar gps space segment/navigation user interfaces," *IS-GPS-200D*, 2006, Revision D.

[9] Proakis J.G., *Digital Communications*, McGraw-Hill Series in Electrical and Computer Engineering, Boston, Massachusetts, third edition, 1995.

[10] Holmes J.K., Chen C.C., "Acquisition time performance of pn spread-spectrum systems," *IEEE Trans. on Commun.*, vol. 25, no. 8, pp. 778–784, Aug. 1977.

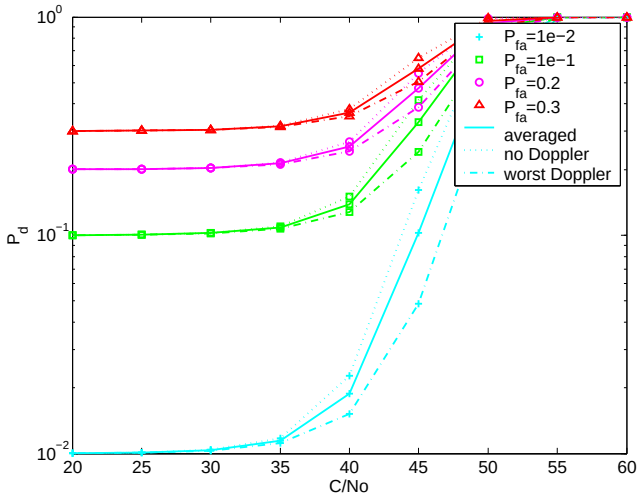

(a) $P_{d,1peak}$ for $P = N = 32$

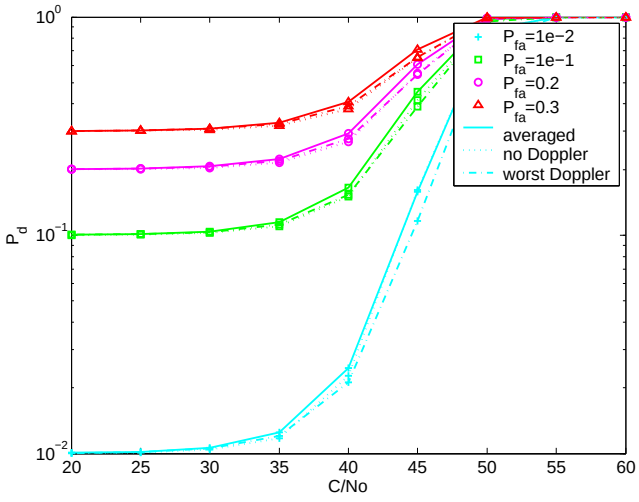

(b) $P_{d,1peak}$ for $P = P_{opt} = 17$

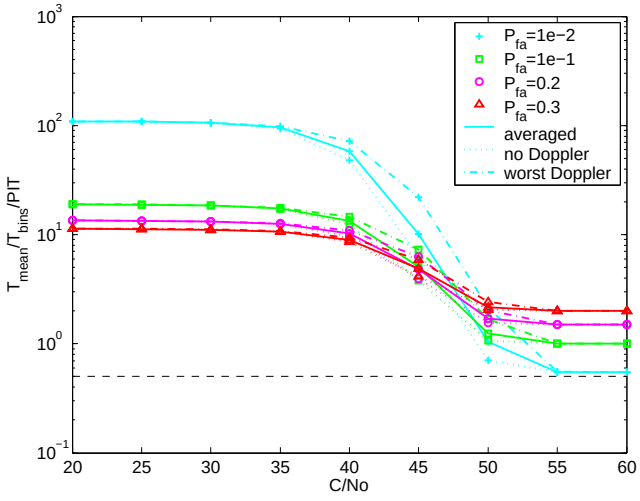

(c) $T_{acqu,1peak}$ for $P = N = 32$

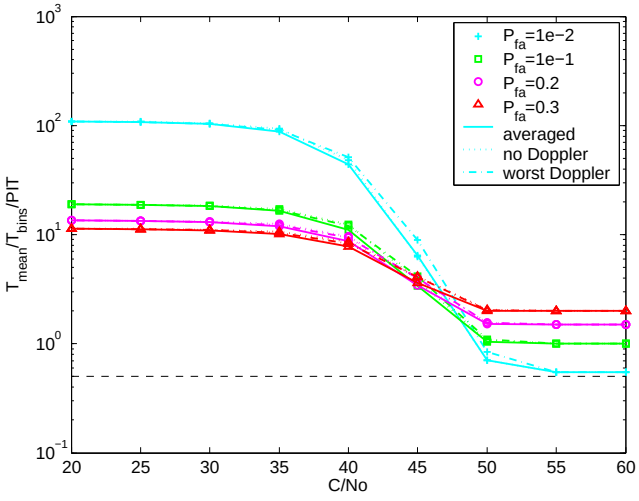

(d) $T_{acqu,1peak}$ for $P = P_{opt} = 17$

Fig. 13 Effect of zero padding (optimal PCMF) for parallel space search architecture: PIT=1ms; N=32.

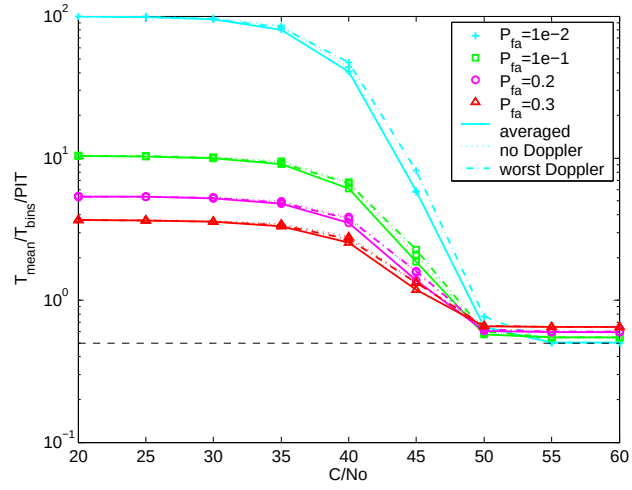

(a) $T_{acqu,1peak}$ for $K = 1$

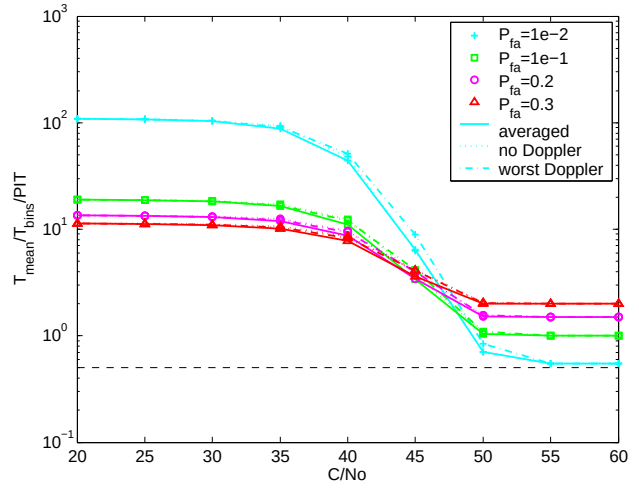

(b) $T_{acqu,1peak}$ for $K = 10$

Fig. 14 Effect of penalty factor K for parallel space search architecture: PIT=1ms; N=32; P=P_{opt}=17.

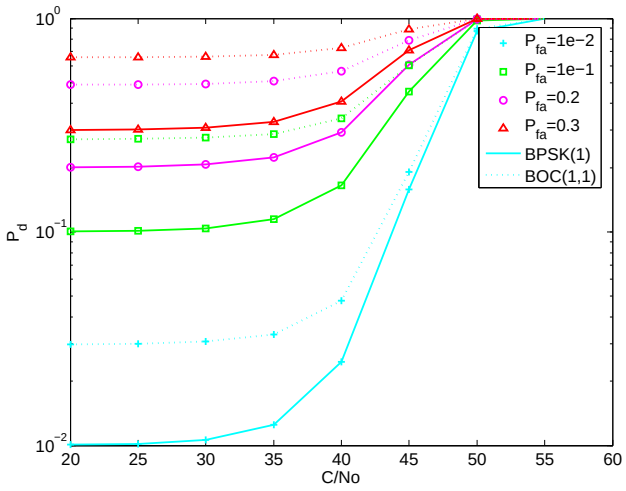

(a) $P_{d,1peak}$ (solid) vs. $P_{d,BOC(1,1)}$ (dashed)

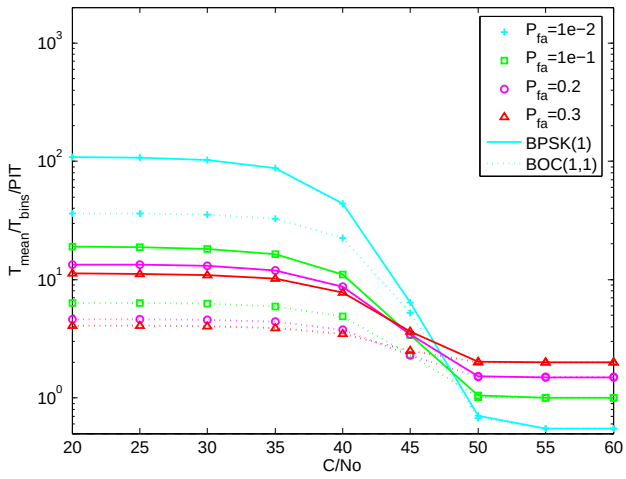

(b) $T_{acqu,1peak}$ (solid) vs. $T_{acqu,BOC(1,1)}$ (dashed)

Fig. 15 Effect of full BOC(1,1) vs. single lobe acquisition for parallel space search: PIT=1ms; N=32; P=P_{opt}=17, K=10.

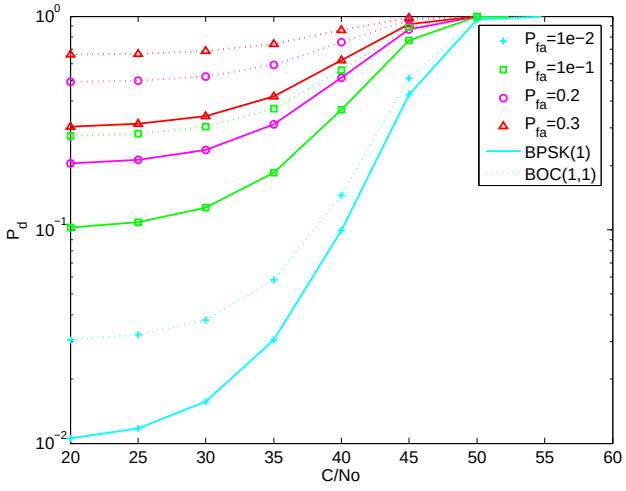

(c) $P_{d,1peak}$ (solid) vs. $P_{d,BOC(1,1)}$ (dashed

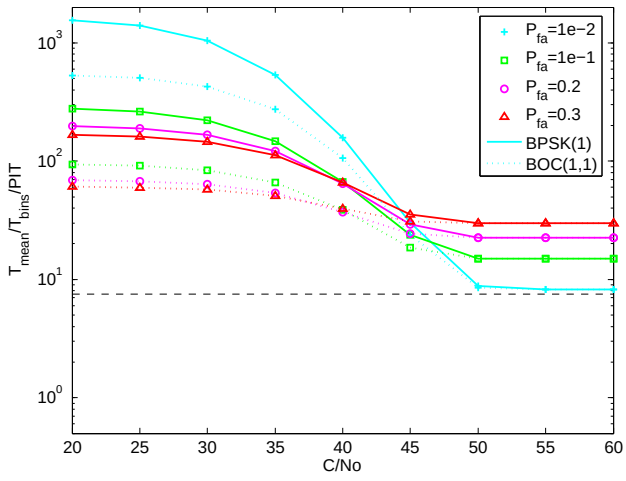

(d) $T_{acqu,1peak}$ (solid) vs. $T_{acqu,BOC(1,1)}$ (dashed)

Fig. 16 Effect of full BOC(1,1) vs. single lobe acquisition for serial search architecture: PIT=1ms; K=10.